Felsic melt migration via porous flow – a numerical modeling approach

Petra Maierová, Pavlína Hasalová, Karel Schulmann

EGU21-5703

Motivation

Contrasting styles of melt migration through the crust:

- segregation and migration of melt through interconnected network of veins and/or melt-rich layers
- typical in metasedimentary rocks

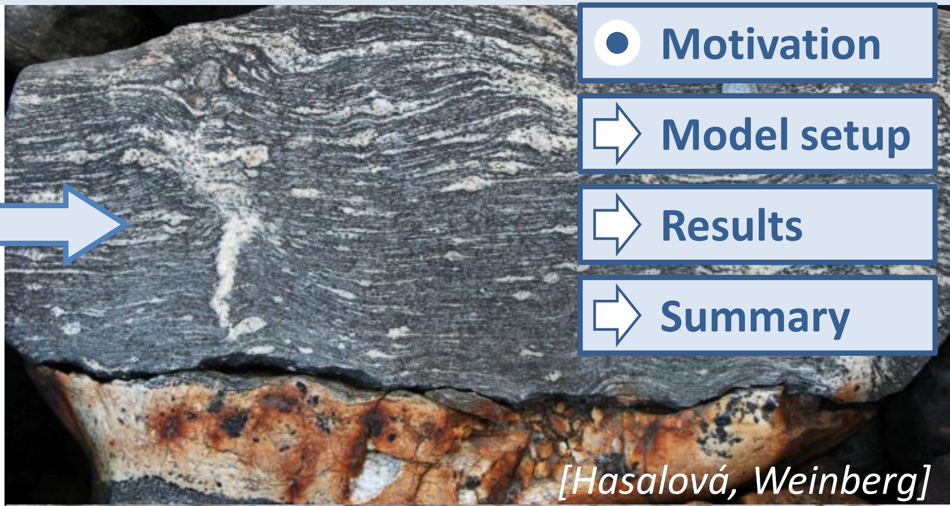

[Hasalová, Weinberg]

- pervasive melt migration along grain boundaries, equilibration with the host rock, lack of segregation structures
- **→ metaigneous migmatites in the Bohemian Massif** formed from orthogneiss interacting with migrating melt

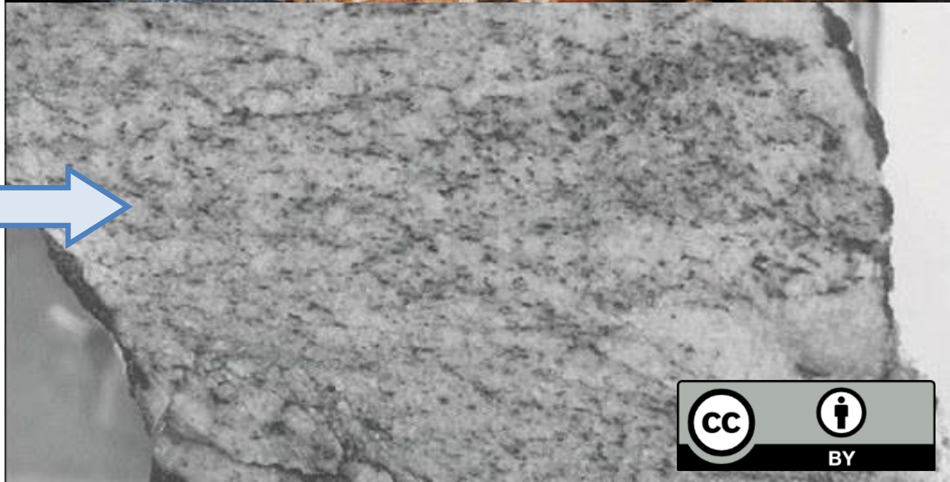

Motivation – observed sequence of migmatites I

- a continuous sequence of texturally, geochemically and compositionally different migmatites
- changes in microstructure from monomineralic recrystallized bands to isotropic distribution resembling the texture of granite

gradual change by percolating melt

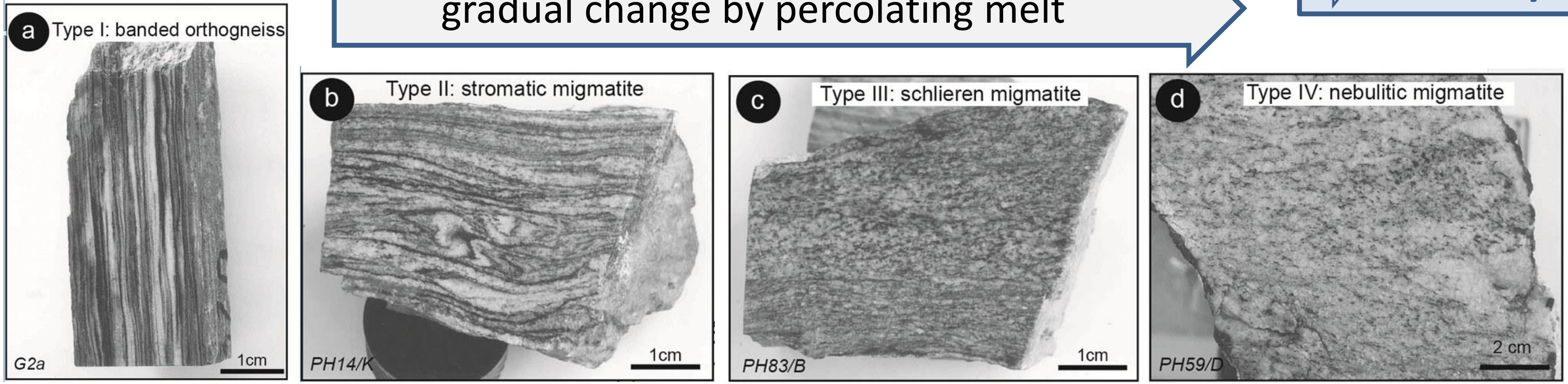

- formed from orthogneiss by open-system melt infiltration → further geological data
  [Hasalová et al., 2008a,b,c]

Motivation – observed sequence of migmatites II

- increasing amount of small interstitial grains of felsic minerals – crystallized from granitic melt
- changes in whole rock composition towards more silica-rich
- changes in trace and RE elements
- recorded PT conditions change from 800°C at ~8 kbar to 700°C at ~5 kbar
- U-Pb and monazite dating shows 10 Myr duration of the process
- small melt fraction (<10 mol.%)
- calculated melt composition: granitic with 7–8 wt.% of water
- [Hasalová et al., 2008a,b,c]

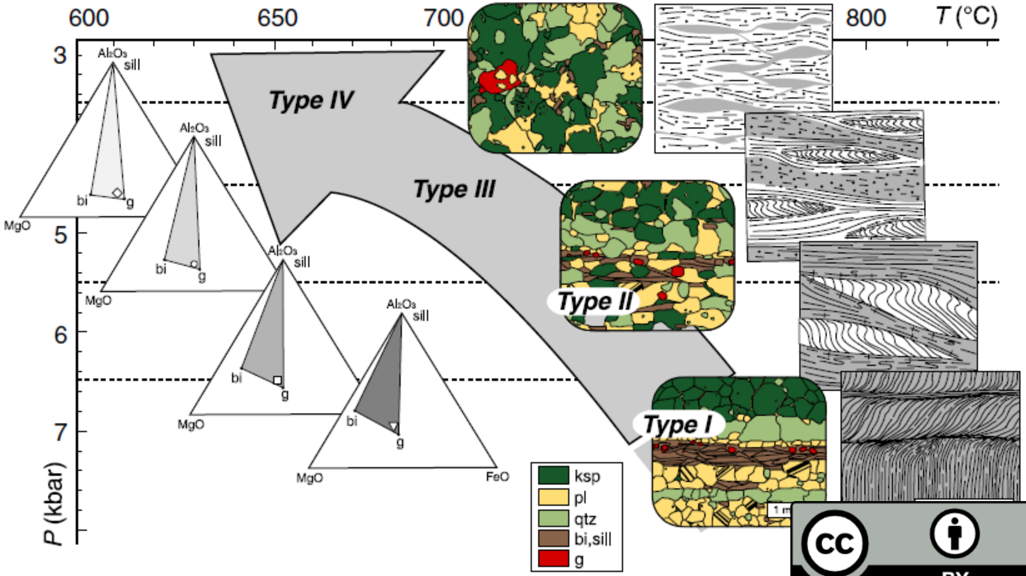

Motivation – questions and goals

Questions

- At what conditions can felsic melt migrate along grain boundaries without segregating to veins or other conduits, as observed in the studied sequence of migmatites?
- What are possible styles of melt migration in the crust?
- Can numerical models of two-phase flow mimic these processes?

Goals

- Set up → a model of melting and melt migration in crustal rocks in orogens.
- Compare → evolution of models with different material parameters, corresponding to different crustal rocks, in different temperature conditions.
- Compare obtained models with → geological data.

Model setup

- computations were done using the **ASPECT code** version 2.2.0 [Kronbichler et al., 2012; Dannberg and Heister, 2016; Heister et al., 2017; Bangerth et al., 2020]
- **two phase flow** (solid matrix and melt), **temperature evolution**, **melting and freezing** → equations
- **crustal-scale model** focused on deformation at km-scale; grain–to–vein scale described only by the rock permeability
- only **viscous** deformation (no description of fracturing)
- →model domain
- adaptive refinement – finer resolution in sites where melt is present
- operator splitting – shorter time step for computation of reaction terms in solved equations
- **crust-like material properties** →thermal parameters, radiogenic heat sources, → density, →shear viscosity of solid matrix, → porosity dependence of viscosity (bulk viscosity of solid matrix), →viscosity of melt, →permeability, →melting parametrization using solidus and liquidus temperatures

Model setup – equations

- conservation of mass (*f*luid and *s*olid) using porosity ϕ, Darcy's law

$$\begin{aligned} \frac{\partial \rho_s(1-\phi)}{\partial t} + \nabla \cdot [\rho_s(1-\phi)\mathbf{u}_s] &= -\Gamma \\ \frac{\partial \rho_f \phi}{\partial t} + \nabla \cdot [\rho_f \phi \mathbf{u}_f] &= \Gamma \end{aligned}$$

$$\mathbf{u}_f = \mathbf{u}_s - \frac{K_D}{\phi}(\nabla p_f - \rho_f \mathbf{g})$$

- conservation of momentum

$$-\nabla \cdot \left[2\eta\left(\dot{\epsilon} - \frac{1}{3}(\nabla \cdot \mathbf{u}_s)\mathbf{I}\right)\right] + \nabla p_f + \nabla p_c = \rho \mathbf{g}$$

- compaction pressure

$$p_c := (1-\phi)(p_s - p_f) = -\eta_b(\nabla \cdot \mathbf{u}_s)$$

- heat equation including radiogenic heating and latent heat of melting

$$\phi \rho_f c_p \left(\frac{\partial T}{\partial t} + \mathbf{u}_f \cdot \nabla T\right) + (1-\phi)\rho_s c_p \left(\frac{\partial T}{\partial t} + \mathbf{u}_s \cdot \nabla T\right) - \nabla \cdot k \nabla T = \rho_s H + T \Delta S \Gamma$$

- advection of depletion *D*

$$\frac{\partial D}{\partial t} + \nabla \cdot (D\mathbf{u}_s) = \frac{\Gamma}{\rho_s}$$

Model setup – model domain

- initial and boundary conditions correspond to thick and warm orogenic crust
- initial conditions on temperature: analytical solution for BCs and
  → radiogenic heat sources
- bottom temperature:

  same as initial temperature with an asymmetrically placed Gaussian anomaly of 100–200 °C

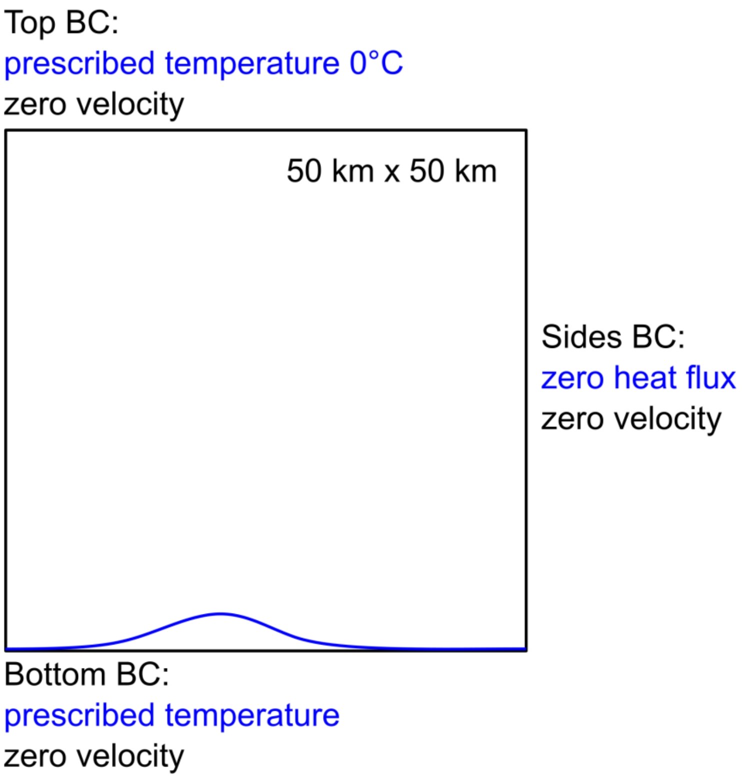

Model setup – thermal parameters, heat sources

- thermal conductivity k_T:

  3 $Wm^{-1}K^{-1}$
- radiogenic heat sources $\rho_s H$:

  exponential decay with depth

  $3x10^{-6}$ Wm^{-3} at the surface

  background productivity $5x10^{-7}$ Wm^{-3} at depth
- latent heat – melting entropy change ΔS:

  300 $Jkg^{-1}K^{-1}$

Model setup – density

$$\rho_s = (\rho_{s0} + \Delta\rho_D D)\left[1 - \alpha(T - T_0)\right]$$

$$\rho_f = \rho_{f0}\left[1 - \alpha(T - T_0)\right]$$

- reference solid density: ρ_{s0} =2700 kg m^{-3}
- depletion dependence: $\Delta\rho_D$ = 200 kg m^{-3}
- reference melt density: ρ_{f0} = 2400 kg m^{-3}
- thermal expansivity: α = 2x10^{-5} K^{-1}

Model setup – shear viscosity of solid

Home | Next | Motivation | Model setup | Results | Summary

$$\eta_s = \eta_0 \exp(-\alpha_\phi \phi) \exp(\alpha_D D) \exp\left(\frac{A_s}{RT}\right)$$

- temperature-dependent relationship, approximation of flow laws for strain rate 10^{-14} s^{-1}
- granite flow law assumed representative for crustal rheology – accounts for weak minerals (mica); similar as wet quartzite flow law; viscosity 10^{18} Pa.s in the lower crust
- depletion dependence of viscosity mimics change to granulitic residuum (felsic granulite) – approx. 2 orders of magnitude increase in viscosity
- → porosity dependence

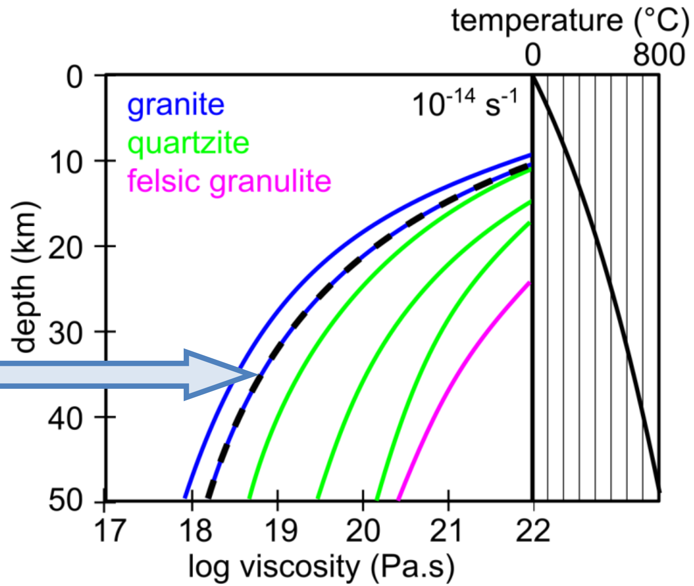

Flow laws for granite [Mackwell et al. 1998; Ranalli, 1995], quartz [Gleason and Tullis, 1995; wet and dry quartz: Ranalli, 1995], felsic granulite [Wilks and Carter, 1990], black dashed – applied flow law (ϕ=0, D=0)

Model setup – porosity dependence of viscosity

$$\eta_s = \quad \eta_0 \exp(-\alpha_\phi \phi) \exp(\alpha_D D) \exp\left(\frac{A_s}{RT}\right)$$

$$\eta_b = \quad \eta_0 \exp\left(-\alpha_\phi \phi\right) \left(10 + \frac{1}{3}\frac{1}{\phi}\right) \exp\left(\frac{A_b}{RT}\right)$$

- reduction of shear viscosity by 1–2 orders of magnitude for porosity ϕ of 0.1–0.2 (10–20% of melt)
- resulting viscosity of ~10^{16} Pa.s agrees with estimates from geophysical data from Tibet and Altiplano [Clark and Royden, 2000; Unsworth et al., 2005]

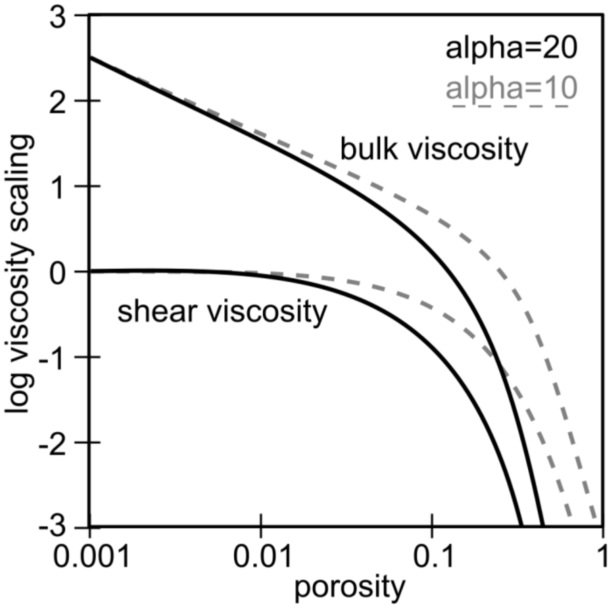

Model setup – viscosity of melt

$$\eta_f = \eta_{f0} \exp\left(\frac{A_f}{RT}\right)$$

- temperature-dependent relationship valid for a given composition and water content

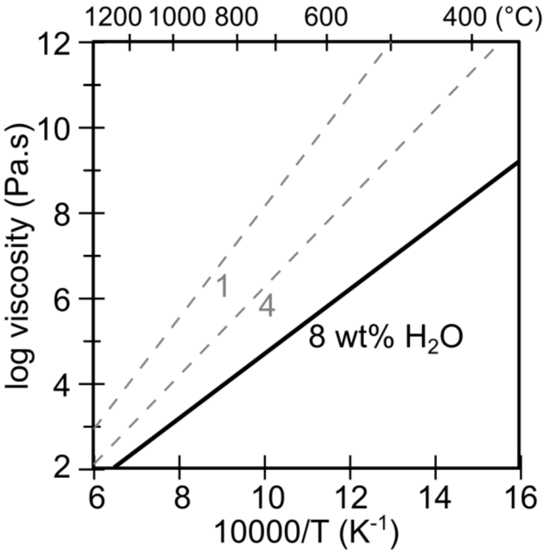

Approximation of experimentally determined melt viscosity [Whittington et al., 2004] for temperature above ~700°C

Model setup – permeability

$$k_\phi = k_0\phi^3 = \frac{1}{C}d^2\phi^3$$

- permeability prefactor *C*=200 [Wark and Watson, 1998]
- spacing of pores *d* corresponds to grain size (melt along grain boundaries) or to spacing of veins or leucosomes [Schmeling et al., 2018]
- different values tested: d=~10^{-3}–10^{-1} m, k_0=10^{-8}–10^{-5} m^2

Model setup – melting parametrization I

- solidus and rock fertility depends on rock composition (dehydration melting) and available fluid (water-fluxed melting) – no simple relationship
- →different parametrizations of melting have to be tested

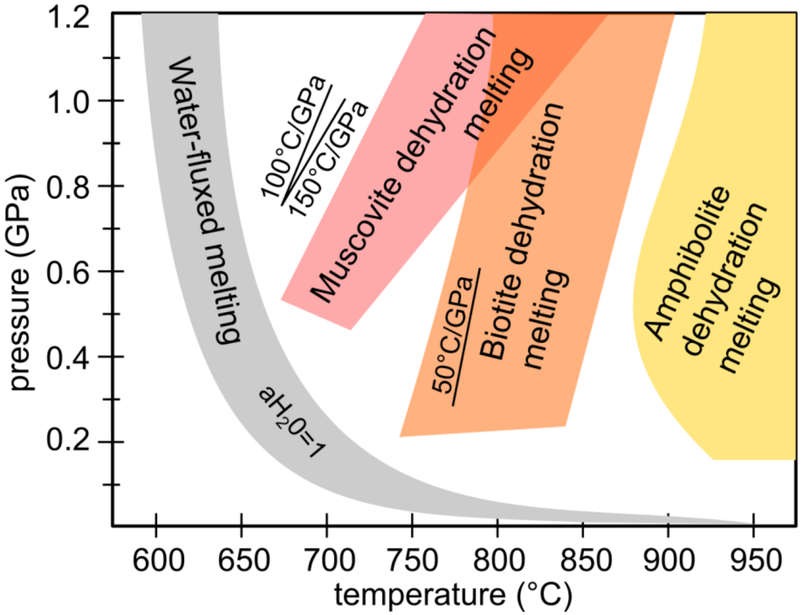

[Weinberg and Hasalová, 2015]

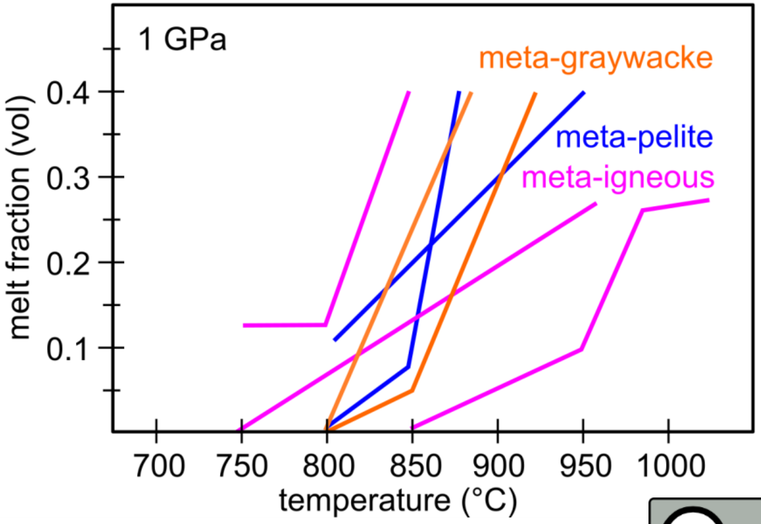

[after Clemens, 2005]

Model setup – melting parametrization II

- solidus and liquidus temperatures depend on pressure and depletion

$$T_\mathrm{S} = T_{\mathrm{S},P=0} + \Delta T_P P + \Delta T_D (D - \phi)$$
$$T_\mathrm{L} = T_\mathrm{S} + \Delta T_\mathrm{LS}$$

- equilibrium melt fraction ϕ_x is used for calculation of melting function Γ

$$\phi_x = \frac{T - T_\mathrm{S}}{T_\mathrm{L} - T_\mathrm{S}} \qquad \Gamma = \rho \frac{\phi_x - \phi}{\Delta t_\mathrm{M}}$$

- prescribed maximum equilibrium melt fraction of 0.3 (30% of melt)
- testing of different parameter values: $T_{S,P=0}$ = 600, 700°C
  ΔT_{LS} = 500, 1000°C
  ΔT_P = 50, 100, 150°C/GPa
  ΔT_D = 0, 300, 400°C

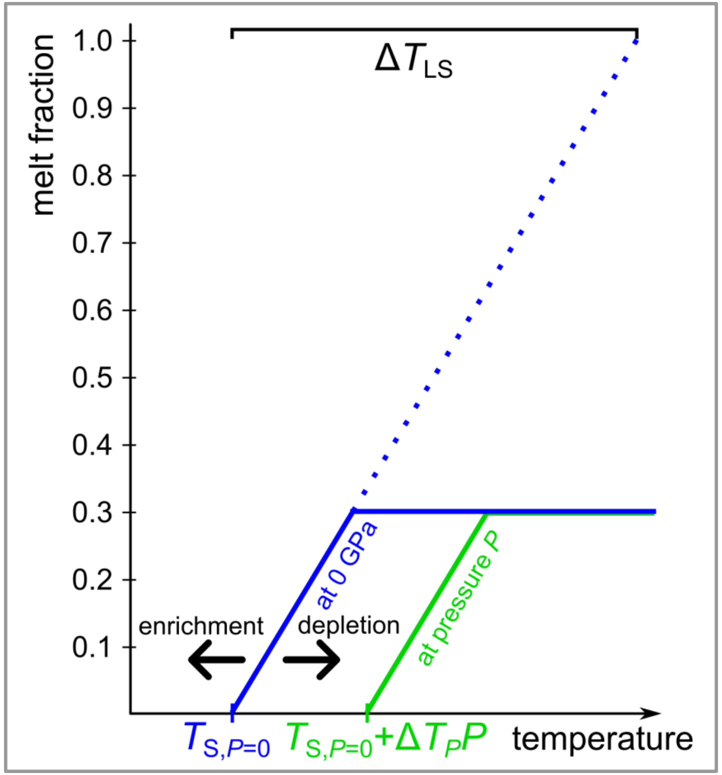

Results

We studied the effect of:

- permeability →high, →medium, →low
- → temperature boundary condition, solidus temperature, solidus-liquidus difference, → pressure and depletion dependence of solidus temperature
- → shear viscosity prefactor, porosity dependence of viscosity

Example of computational grid

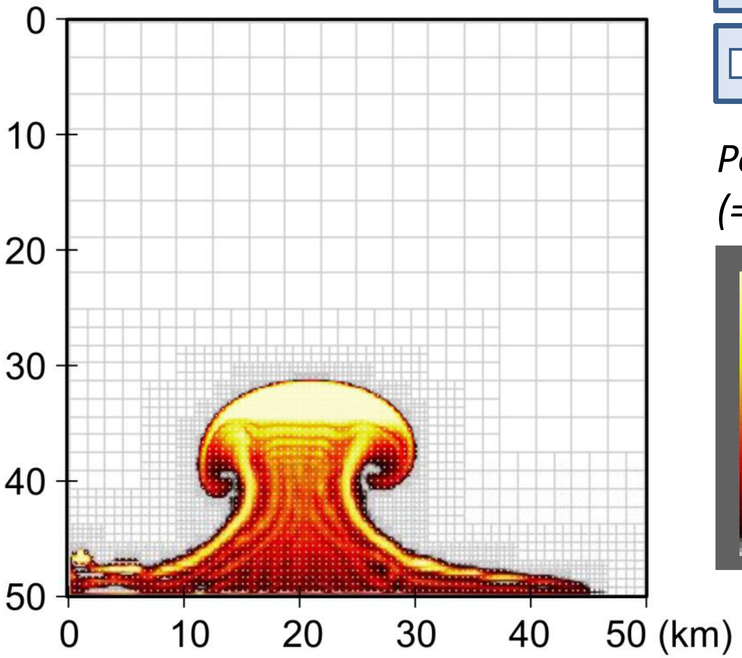

Porosity ϕ
(= melt fraction)

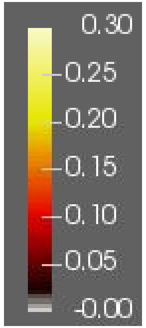

Results – model evolution – high permeability

$k_0=10^{-5}$ m² (d=~5 cm)

- quick melt extraction in vertical porosity channels
- formation of melt-rich zone in middle crust and depleted lower crust

Example: model with $T_{S,P=0}$ = 600°C, ΔT_{LS} = 500°C, ΔT_P = 100°C/GPa, ΔT_D = 300°C and 100°C anomaly at bottom boundary

Porosity ϕ (=melt fraction)

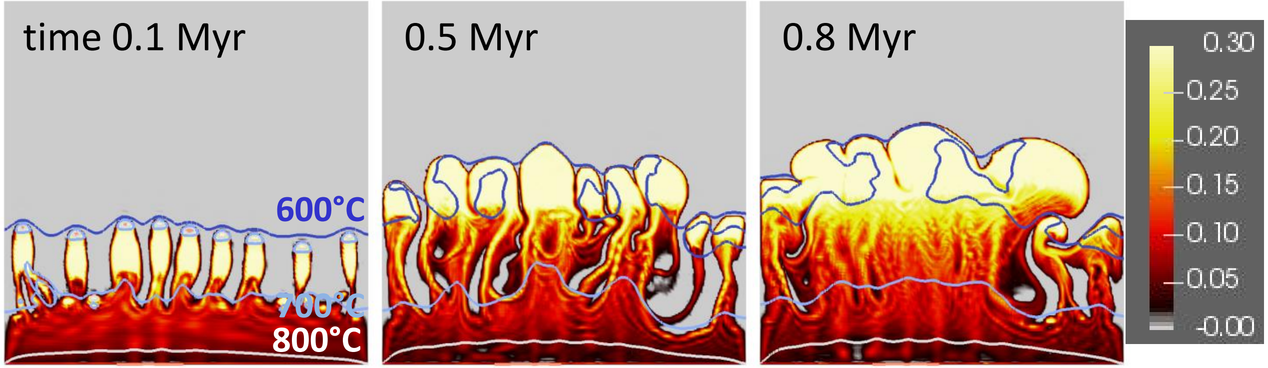

Depletion/enrichment D

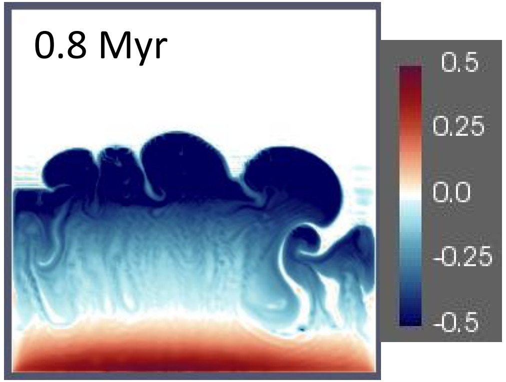

maximum velocity of solid: ~20 cm/yr (in the melt-rich middle crust), ~5 cm/yr in the lower crust
maximum velocity difference between melt and solid: ~50 cm/yr
(at 0.8 Myr)

Results – model evolution – medium permeability

$k_0=10^{-6}$ m^2 (d=~1 cm)

- melt segregates into high-porosity channels
- melt-enhanced convection
- formation of melt-rich zone in middle crust and depleted lower crust

Example: model with $T_{S,P=0}$ = 600°C, ΔT_{LS} = 1000°C, ΔT_P = 100°C/GPa, ΔT_D = 300°C and 100°C anomaly at bottom boundary

Porosity ϕ (=melt fraction)

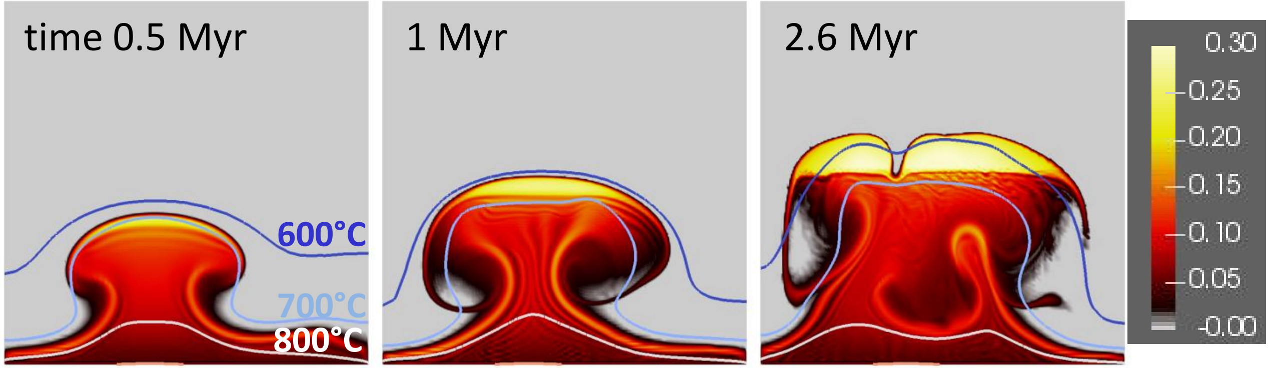

Depletion/enrichment D

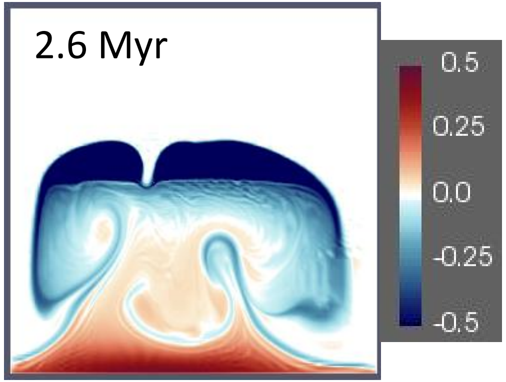

maximum velocity of solid: ~10 cm/yr
maximum velocity difference between melt and solid: ~10 cm/yr (at 2.6 Myr)

Results – model evolution – low permeability

$k_0=10^{-8}$ m^2 (d=~1 mm)

- diapirs form and merge into melt-enhanced convection
- motion of melt with respect to the solid matrix is slow, but for quick deformation (high porosity) it can still reach cm per year

Example: model with $T_{S,P=0}$ = 600°C, ΔT_{LS} = 1000°C, ΔT_P = 100°C/GPa, ΔT_D = 300°C and 100°C anomaly at bottom boundary

Porosity ϕ (=melt fraction)

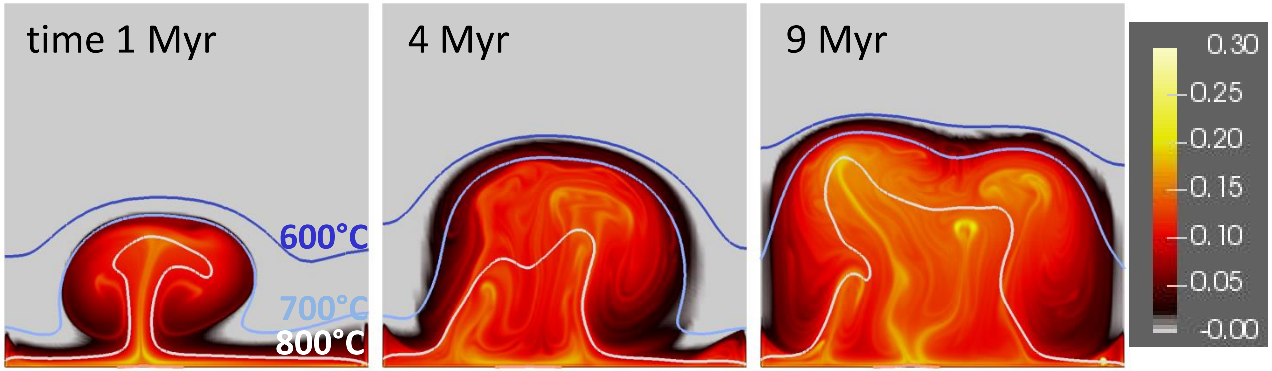

Depletion/enrichment D

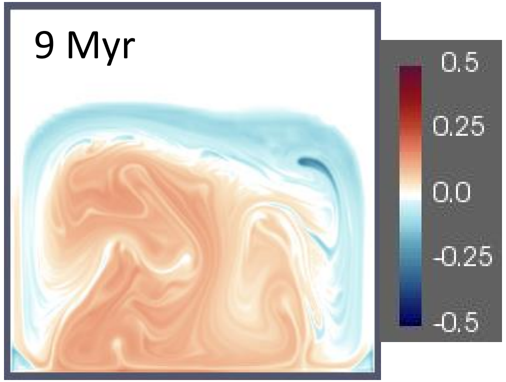

maximum velocity of solid: ~15 cm/yr

maximum velocity difference between melt and solid: ~1 cm/yr (at 9 Myr)

Results – effect of melting parametrization I

Examples of model results – snapshots after 2 Myr of model evolution

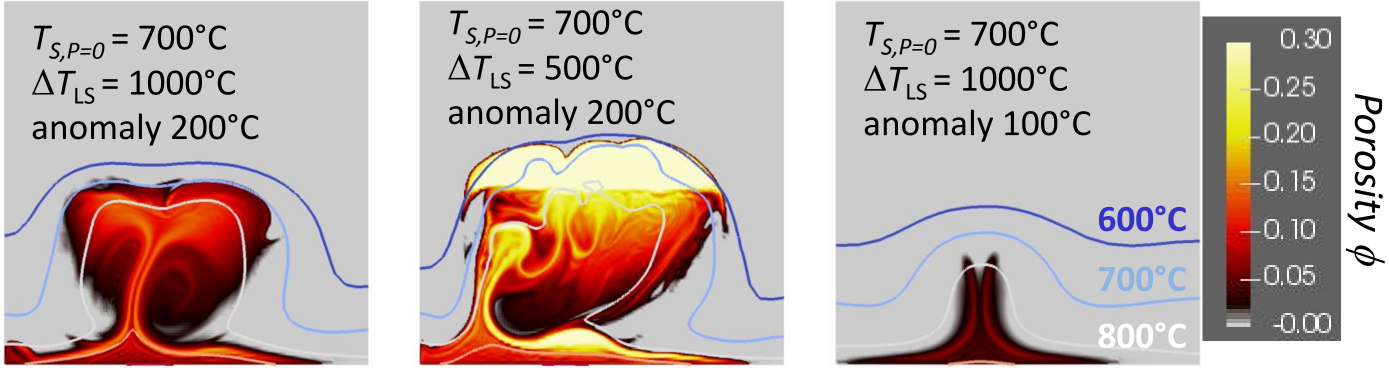

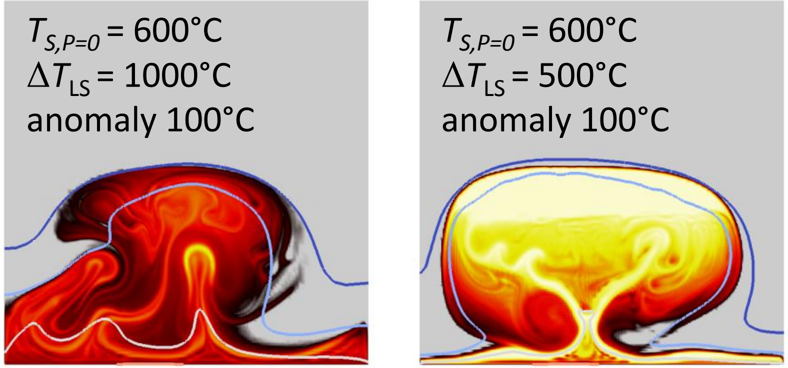

- low solidus, small solidus–liquidus difference, large temperature anomaly at bottom boundary => more melting, melt accumulation in middle crust
- fixed parameters:

  k_0=10^{-7} m^2, ΔT_P = 100°C/GPa, ΔT_D = 300°C

Results – effect of melting parametrization II

Examples of model results – snapshots after 2 Myr of model evolution

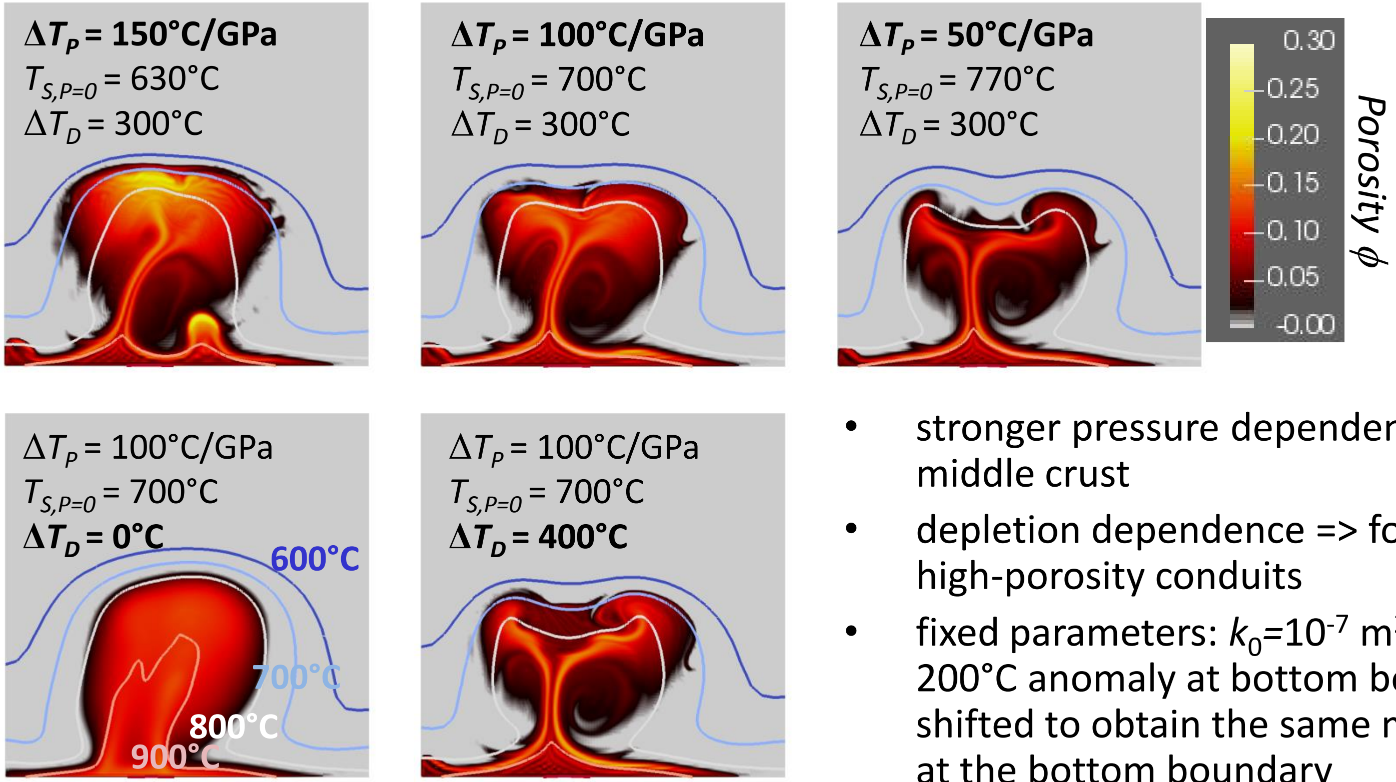

- stronger pressure dependence => more melt in middle crust
- depletion dependence => focusing of melt to high-porosity conduits
- fixed parameters: k_0=10^{-7} m^2, ΔT_{LS} = 1000°C and 200°C anomaly at bottom boundary; solidus shifted to obtain the same melting temperature at the bottom boundary

Results – effect of viscosity

Examples of model results – snapshots after 2 Myr of model evolution

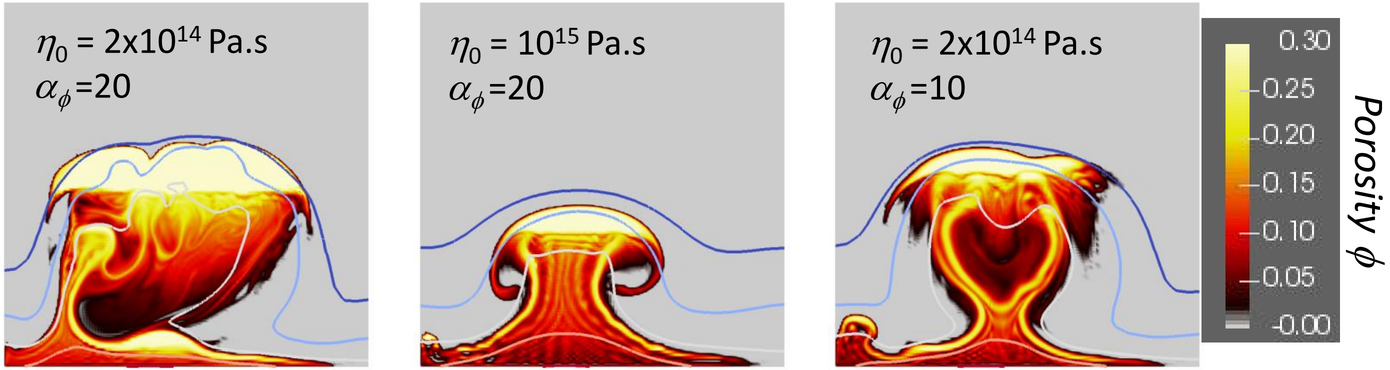

- higher viscosity of the solid matrix => slower deformation, less vigorous convection, relatively more important separation of melt from solid matrix
- fixed parameters:

k_0=10^{-7} m^2, ΔT_{LS} = 500°C, 200°C anomaly at bottom boundary, ΔT_D = 300°C, ΔT_P = 100°C/GPa

Summary – melt migration styles

- We have set up a **numerical model of melting and melt migration** in thickened continental crust.
- The model with different parameters show different styles of melt migration and solid matrix deformation: **diapirism**, melt-enhanced **convection**, km-scale **pulses** of high porosity gathering to melt conduits, vertical **melt conduits**.
- In all models, **melt is efficiently removed from the lower crust**, with or without significant deformation of the matrix.
- In models, where relative motion between melt and matrix is significant, **depleted** lower crust and **enriched** upper–middle crust form.

Summary – metaigneous vs metasedimentary rocks

- Permeability of the solid matrix is the key parameter of the model.
- For a **low permeability** diapirism and convection occur. Velocity of the melt with respect to the matrix is ~1 cm yr^{-1} at maximum.
- Such a low permeability (*d* is the grain size) is expected in the studied Bohemian massif metaigneous migmatites. In comparison with these migmatites, the temperature in the middle crust is still too low and therefore the shallowest level of melting is too deep (observed 10–15 km vs modeled 15–20 km).
- For a **high permeability** melt migrates in pulses and forms high-porosity conduits and zones. Melt segregates more easily and forms a melt-rich middle crust and depleted lower crust in the time scale of less than 1 Myr (depending on model parameters).
- High permeability describes a layered structure (leucosome-mesosome) characteristic for metasediments or to a system of veins.

Summary – limitations and future work

- The applied modeling approach works only for **low to medium melt fractions**. Disintegration of the solid matrix and magmatic flow is not modeled.
- **Ductile matrix rheology** is assumed. Brittle fracturing and elasticity are not taken into account. Anisotropy of the rock, which might be important especially in the case of metasedimentary rocks, is neglected.
- Very **high velocities** – are observed in hot partially-molten crust in models with melt-enhanced convection. It is a direct consequence of the low viscosity prescribed in agreement with geophysical data.
- **Gravity is the driving force** for deformation and melt migration in our models. Stresses induced by plate motions and variable surface topography may contribute to deformation and influence the style of melt migration.
- The applied **parametrization of melting is rather artificial** – a more natural parametrization based on the rock composition (content of muscovite and biotite) should be tested.
- Note: Small-scale melt segregation (or its absence) is not explained by this model, it is rather a result of initial heterogeneity or anisotropy of the rock.

References and Acknowledgements I

Home Next

This contribution was funded by the Grant Agency of the Czech Republic – grant GAČR EXPRO GX19-27682X.

We thank the Computational Infrastructure for Geodynamics (geodynamics.org) which is funded by the National Science Foundation under award EAR-0949446 and EAR-1550901 for supporting the development of ASPECT.

References

Bangerth et al. (2020). ASPECT v2.2.0. (version v2.2.0). Zenodo. https://doi.org/10.5281/ZENODO.3924604.
Bangerth et al. (2020). ASPECT: Advanced Solver for Problems in Earth's ConvecTion, User Manual. https://doi.org/10.6084/m9.figshare.4865333
Clark and Royden (2000). Topographic ooze: Building the eastern margin of Tibet by lower crustal flow. Geology, 28(8), 703-706.
Dannberg and Heister (2016). Compressible Magma/mantle Dynamics: 3-D, Adaptive Simulations in ASPECT. Geophysical Journal International 207 (3) 1343–1366.
Gleason and Tullis (1995). A flow law for dislocation creep of quartz aggregates determined with the molten salt cell. Tectonophysics, 247(1-4), 1–23.
Hasalová et al. (2008a). From orthogneiss to migmatite: geochemical assessment of the melt infiltration model in the Gföhl Unit (Moldanubian Zone, Bohemian Massif). Lithos, 102(3-4), 508-537.
Hasalová et al. (2008b). Origin of migmatites by deformation-enhanced melt infiltration of orthogneiss: A new model based on quantitative microstructural analysis. Journal of Metamorphic Geology, 26(1), 29-53.

References and Acknowledgements II

Home

Hasalová et al. (2008c). Transforming mylonitic metagranite by open-system interactions during melt flow. Journal of Metamorphic Geology, 26(1), 55-80.

Heister et al. (2017). High Accuracy Mantle Convection Simulation through Modern Numerical Methods – II: Realistic Models and Problems. Geophysical Journal International 210 (2), 833–851.

Kronbichler et al. (2012). High Accuracy Mantle Convection Simulation through Modern Numerical Methods. Geophysical Journal International 191 (1), 12–29.

Mackwell et al. (1998). High-temperature deformation of dry diabase with application to tectonics on Venus. Journal of Geophysical Research: Solid Earth, 103(B1), 975-984.

Ranalli (1995). Rheology of the Earth. Springer Science & Business Media.

Schmeling et al. (2012). Effective shear and bulk viscosity of partially molten rock based on elastic moduli theory of a fluid filled poroelastic medium. Geophysical Journal International, 190(3), 1571-1578.

Schmeling et al. (2019). Modelling melting and melt segregation by two-phase flow: new insights into the dynamics of magmatic systems in the continental crust. Geophysical Journal International, 217(1), 422-450.

Unsworth et al. (2005). Crustal rheology of the Himalaya and Southern Tibet inferred from magnetotelluric data. Nature, 438(7064), 78-81.

Weinberg and Hasalová (2015). Water-fluxed melting of the continental crust: A review. Lithos, 212, 158-188.

Wark and Watson (1998). Grain-scale permeabilities of texturally equilibrated, monomineralic rocks. Earth and Planetary Science Letters, 164(3-4), 591-605.

Wilks and Carter (1990). Rheology of some continental lower crustal rocks. Tectonophysics, 182(1-2), 57-77.

Whittington et al. (2005). Experimental temperature-X (H2O)-viscosity relationship for leucogranites and comparison with synthetic silicic liquids. Geol. Soc. Am. Spec. Pap, 389, 59-71.